Signal Processing 130 (2017) 279–288

Contents lists available at ScienceDirect

Signal Processing

journal homepage: www.elsevier.com/locate/sigpro

Radar network topology optimization for joint target position and velocity estimation

Inna Ivashko *, Geert Leus, Alexander Yarovoy

Delft University of Technology, 2628 CD Delft, The Netherlands

ARTICLE INFO

Article history:
Received 7 March 2016
Received in revised form
24 May 2016
Accepted 5 July 2016
Available online 9 July 2016

Keywords:
Radar network
Topology optimization
Greedy optimization
Frame potential
Log-determinant

ABSTRACT

In this paper, we tackle the problem of selecting the radar node positions to provide an estimate of the target state vector with a prescribed accuracy. The topology optimization problem is formulated as selection of a fixed number of radar node positions from a set of available ones, where the radar observations are modeled by a general non-linear model. We further propose a topology optimization framework for the simultaneous estimation of the multi-modal parameter vector. In particular, the task of joint position and velocity estimation is considered. The feasibility of the proposed approach is demonstrated for several cost functions, namely the frame potential as well as the log-determinant and maximum eigenvalue of the error covariance matrix.

1. Introduction

In recent years the radar sensor application area experiences a booming growth. Radar sensors, which are becoming much smaller and cheaper due to advances in microwave technology, are widely used for different applications that require 24/7 area monitoring, such as ground/air traffic control, environment monitoring (precipitation, temperature, pollution), patient monitoring, to list a few [1–3]. The replacement of a single complex radar with a network of simple radar units that enclose the observation area enables a higher detection probability and evaluation of 3D target data [4]. Although the idea of the simultaneous exploitation of data from multiple radar nodes has been discussed several decades ago [5,4,6], radar networks have become widely experimentally studied over the last few years due to advances on high-data rate communications and signal processing capabilities, which made it possible at low costs to synchronize radar nodes and process simultaneously (and in real time) their output [7,8].

While the power budget and the waveform parameters determine the performance of a single radar node [9], the overall performance of a radar network is determined by the number of nodes and their spatial locations [10]. Along with the single radar node characteristics, these network parameters define the total coverage area in terms of predefined detection and accuracy of the target parameter estimates, as well as the overall robustness of the system. Therefore, an efficient exploitation of the radar network requires optimal node allocation. The latter can be considered either as a real-time or off-line design task, depending on the particular application. The selection of spatial positions of radar nodes is one of the key tasks in radar network resource allocation. It aims to achieve the optimal system performance with minimum system costs.

1.1. Prior work

Different techniques for spatial radar (sensor) placement are presented in the literature [11–15]. In general, they are aimed at tackling two types of optimization problems:

1. Selection of the minimal number of radar nodes to meet some prescribed system performance requirements.
2. Selection of a fixed and known amount of radar nodes that corresponds to the best possible system performance.

Depending on the mission, different performance metrics are used for the system design. The three most common functionalities of the radar are target detection, state vector estimation, and tracking. Previous studies mostly focus on the selection of the radar network configuration that ensures only accurate target localization. However, a number of radar applications require

* Corresponding author.
E-mail addresses: I.Ivashko@tudelft.nl (I. Ivashko), G.J.T.Leus@tudelft.nl (G. Leus), A.Yarovoy@tudelft.nl (A. Yarovoy).

http://dx.doi.org/10.1016/j.sigpro.2016.07.010
0165-1684/

knowledge of the full target state vector, which includes not only the location, but also the velocity of the target at each time instant [16]. Additionally, the use of the Doppler shift provides higher detection probability in a strong clutter [17]. Topology optimization for the joint position and velocity vector estimation of a ground moving target (GMT) using pulse Doppler radars on-board unmanned aerial vehicles (UAVs) was considered in [18,16]. However, the assumption made in [18] is related to the constant accuracy of the UAV measurements and does not allow for an optimal solution in terms of signal-to-noise ratio (SNR). Both approaches from [18] and [16] explore the mobility of the sensors, which requires a real-time optimization.

In this paper, we focus on the off-line problem of radar node positions selection to satisfy prescribed accuracy requirements of the target state vector estimation. The estimation accuracy measures are often chosen to be scalar functions of the error covariance matrix, such as 1) the maximum eigenvalue (E-optimality); 2) the trace (A-optimality); and 3) the log-determinant (D-optimality). Other measures, like mutual information, entropy, and cross-entropy, are frequently used as well [19,20]. The sensor selection problem is combinatorial in nature. Therefore, different optimization techniques are used to solve it in polynomial time. For example, convex optimization methods, which are based on the relaxation of the Boolean constraint $\{0, 1\}^N$ on the selection coefficients, were shown to perform well in terms of mean square error (MSE). At the same time, these methods imply a high computational cost. In contrast to convex methods, greedy algorithms have a linear complexity. While the first class of methods requires the cost function to be convex, the second one requires its submodularity. In particular, the log-determinant, the mutual information, and the entropy were shown to be submodular functions. Another submodular function, namely the frame potential (FP), which is a measure for the orthogonality of the rows of the measurement matrix, was introduced in [13] as a proxy for the mean square error. Together with a low computational complexity, the FP-based greedy algorithm sometimes shows a competitive performance with convex optimization [13].

1.2. Our contributions

In this work, we tackle the problem of selecting the optimal radar node positions, which provide the most accurate estimation of the target parameters, namely the position and velocity vectors. The radar network is assumed to operate in a static mode, i.e. with fixed node positions. We develop a generic framework for topology optimization based on non-linear measurement models. Both the frame potential and the log-determinant (LD) of the error covariance matrix are used as performance metrics. These cost functions were shown to be submodular, which allows one to use greedy optimization algorithms ensuring a near-optimal performance and a low computational complexity [13,21]. We redesign the FP and the LD to our specific non-linear model, where the parameter vector can take any value from the known parameter space and can be represented by entries of different modalities (e.g., range and velocity). The developed theoretical framework is applied to the problem of topology optimization for a frequency-modulated continuous-wave (FMCW) radar network for only target position vector estimation as well as for the simultaneous position and velocity estimation. Closed-form expressions of the FP and the LD cost functions for an FMCW radar network are derived. The radar power budget and the waveform parameters are incorporated in both performance metrics, which provide both angular- and range-dependent solutions. The developed technique does not ensure a Doppler coverage model, like the one developed in [17]. This means that although the target might be Doppler covered, the accuracy of the velocity vector estimation might be very low and depends on its position (e.g., on the baseline between two radars).

The rest of the paper is organized as follows. The measurement model, the cost functions and the optimization algorithm are introduced in Section 2. The extension of the optimization approach to the case with multi-modal target parameters is provided in Section 3. Section 4 presents closed-form expressions of the FP and the LD cost functions for an FMCW radar network with details provided in Appendix A. Section 5 presents the results on topology optimization for an FMCW radar network. Section 6 concludes the paper. We use the following notations. $\boldsymbol{a}$ and $\boldsymbol{A}$ denote a vector and matrix, respectively. $E(\cdot)$ denotes the statistical average. $(\cdot)^T$ denotes matrix transpose. $(\cdot)^*$ is the complex conjugate. $(\cdot)^\dagger$ is the Hermitian operator. $\mathrm{tr}\{\cdot\}$ denotes the trace of the matrix. $\mathrm{frac}(\cdot)$ is the fractional part of a real number.

2. General framework

2.1. Non-linear measurement model

We consider a general non-linear measurement model for a set of N possible radar positions

$$\boldsymbol{y} = \boldsymbol{f}(\boldsymbol{\alpha}) + \boldsymbol{\xi}, \tag{1}$$

where $\boldsymbol{y} \in \mathbb{R}^{NQ}$ is the vector of accumulated measurements with Q being the number of accumulated signal samples per integration time in a single radar, $\boldsymbol{\alpha} \in \mathbb{R}^K$ is the vector of parameters to be estimated, $\boldsymbol{f}$ is the non-linear vector function, and $\boldsymbol{\xi} \in \mathbb{R}^{NQ}$ is the measurement noise. We formulate the topology optimization problem as the selection of the L most informative radar positions from the N available ones, where L is known a priori. The sets of selected and available radar positions are defined as $\mathcal{L} = \{i_1, \ldots, i_L\}$ and $\mathcal{N} = \{1, \ldots, N\}$, respectively, where $\mathcal{L} \subseteq \mathcal{N}$ and thus $L \leq N$. For the sake of simplicity, we assume that all radars in the network have the same operating parameters, although this assumption can easily be relaxed.

Since the error covariance matrix for a non-linear measurement model depends on the parameter vector $\boldsymbol{\alpha}$, all covariance-based cost functions depend on $\boldsymbol{\alpha}$ as well [22]. Therefore, we grid the parameter space and perform the optimization considering the complete set of M grid points $\{\boldsymbol{\alpha}_1, \boldsymbol{\alpha}_2, \ldots, \boldsymbol{\alpha}_M\}$. Furthermore, we linearize the model (1) around every grid point $\boldsymbol{\alpha}_m$ applying a first-order Taylor series expansion,

$$\boldsymbol{y} \approx \boldsymbol{f}(\boldsymbol{\alpha}_m) + \boldsymbol{G}_m^{(\mathcal{N})}(\boldsymbol{\alpha} - \boldsymbol{\alpha}_m) + \boldsymbol{\xi}, \tag{2}$$

where the entries of the matrix $\boldsymbol{G}_m^{(\mathcal{N})} \in \mathbb{R}^{NQ \times K}$ are $\left[\boldsymbol{G}_m^{(\mathcal{N})}\right]_{(n-1)Q+q,k} = \left.\frac{\partial f_{(n-1)Q+q}(\boldsymbol{\alpha})}{\partial \alpha_k}\right|_{\boldsymbol{\alpha}=\boldsymbol{\alpha}_m}$; $q = 1, \ldots, Q$; $n = 1, \ldots, N$; $k = 1, \ldots, K$; and $m = 1, \ldots, M$.

In the presence of zero-mean i.i.d. Gaussian noise with variance σ^2, the mean square error, which is equal to the Cramér–Rao lower bound, of the estimate of $\boldsymbol{\alpha}_m$ based on a set $\mathcal{L}$ of selected radars is given by:

$$\mathrm{MSE} = \mathrm{E}(\|\boldsymbol{\alpha}_m - \hat{\boldsymbol{\alpha}}_m\|_2^2) = \sigma^2 \sum_{k=1}^{K} \frac{1}{\lambda_{m,k}}, \tag{3}$$

where $\lambda_{m,k}$ is the kth eigenvalue of the matrix

$\boldsymbol{T}_m^{(\mathcal{L})} = \boldsymbol{G}_m^{\dagger(\mathcal{L})}\boldsymbol{G}_m^{(\mathcal{L})} \in \mathbb{R}^{K\times K}$, with matrix $\boldsymbol{G}_m^{(\mathcal{L})} \in \mathbb{R}^{LQ\times K}$ such that $\left[\boldsymbol{G}_m^{(\mathcal{L})}\right]_{(l-1)Q+q,k} = \left[\boldsymbol{G}_m^{(\mathcal{N})}\right]_{(i_l-1)Q+q,k}$.

The MSE has many local minima in the optimal selection vector, and therefore cannot be efficiently optimized. Popular proxies to the MSE are the maximum eigenvalue and the log-determinant of the error covariance matrix, as well as the frame potential. In particular, the FP and the LD were shown to be monotonic submodular functions [13,21], while the MSE is not. The submodularity of the function is related to the concept of diminishing returns and means the following. For two sets $\mathcal{X}$ and $\mathcal{Y}$ such that $\mathcal{X} \subset \mathcal{Y} \subset \mathcal{N}$ and element $j \in \mathcal{N} - \mathcal{Y}$, the function $f(\cdot)$ is submodular if

$$f(\mathcal{X}+j) - f(\mathcal{X}) \geq f(\mathcal{Y}+j) - f(\mathcal{Y}). \tag{4}$$

This property together with monotonicity allows one to reach a near-optimal solution with greedy algorithms [23]. Moreover, greedy algorithms have a linear complexity in the size of the problem, and therefore are of particular interest for large-scale problems. Next, we develop the FP and the LD for the defined general non-linear measurement model (1) with an extension to the case of multi-modal parameter vectors.

2.2. Cost functions and optimization algorithm

We modify the definition of the frame potential given in [13] to the model with Q measurements accumulated per integration time in each of the radars from the set $\mathcal{L}$:

$$\mathrm{FP}_m(\mathcal{L}) = \sum_{i,j\in\mathcal{L}} \left|\mathrm{tr}\left\{\boldsymbol{G}_m^{(i)}\boldsymbol{G}_m^{(j)\dagger}\right\}\right|^2, \tag{5}$$

where $\boldsymbol{G}_m^{(i)} \in \mathbb{R}^{Q\times K}$ is the submatrix of $\boldsymbol{G}_m^{(\mathcal{N})}$ given by $\left[\boldsymbol{G}_m^{(i)}\right]_{q,k} = \left[\boldsymbol{G}_m^{(\mathcal{N})}\right]_{(i-1)Q+q,k}$. As was shown in [13], the minimization of the FP is related to the minimization of the MSE. While the MSE function has many local minima, the use of the FP allows for a near optimal solution in terms of the minimum MSE. In order to perform a joint optimization over all grid points of the parameter space, the FP in (5) is modified to a weighted FP as [24]

$$\mathrm{FP}(\mathcal{L}) = \sum_{m=1}^{M} p_m \mathrm{FP}_m(\mathcal{L}), \tag{6}$$

where $p_m > 0$ is the weight that represents the probability that the true $\boldsymbol{\alpha}$ lies on the grid point $\boldsymbol{\alpha}_m$; $\sum_{m=1}^{M} p_m = 1$.

Related to the weighted FP, the following monotonic submodular cost function is maximized

$$F(\mathcal{S}) = \mathrm{FP}(\mathcal{N}) - \mathrm{FP}(\mathcal{N}\backslash\mathcal{S}), \tag{7}$$

where $\mathcal{S} = \mathcal{N}\backslash\mathcal{L}$.

The log-determinant of the error covariance matrix, which indicates the log-volume of the confidence ellipsoid is given by

$$\mathrm{LD}_m(\mathcal{L}) = \mathrm{logdet}\left[\sum_{i\in\mathcal{L}} \mathrm{tr}\left\{\boldsymbol{G}_m^{(i)}\boldsymbol{G}_m^{(i)\dagger}\right\}\right]^{-1}. \tag{8}$$

The weighted log-determinant over the set of grid points from the parameter space is then modified to

$$\mathrm{LD}(\mathcal{L}) = \sum_{m=1}^{M} p_m \mathrm{logdet}\left[\sum_{i\in\mathcal{L}} \mathrm{tr}\left\{\mathbf{G}_m^{(i)}\mathbf{G}_m^{(i)\dagger}\right\}\right]^{-1}. \tag{9}$$

In order to apply greedy optimization, the LD-based cost has to be monotonic and submodular and is given by [25]

$$\mathrm{F}(\mathcal{L}) = -\sum_{m=1}^{M} p_m \left(\mathrm{logdet}\left[\sum_{i\in\mathcal{L}} \mathrm{tr}\left\{\boldsymbol{G}_m^{(i)}\boldsymbol{G}_m^{(i)\dagger}\right\} + \epsilon\mathbf{I}_K\right]^{-1} + K\log\epsilon\right), \tag{10}$$

where $\epsilon > 0$ is a small positive number, $\mathbf{I}_K$ is the identity matrix of size K, and the term $(K\log\epsilon)$ ensures that the function (10) is zero for an empty set $\mathcal{L}$. The maximization of the function $F(\cdot)$ from (7) corresponds to the removal of $N-L$ rows from the matrix $\boldsymbol{G}_m^{(\mathcal{N})}$, while the maximization of $F(\cdot)$ from (10) corresponds to the accumulation of L rows that form the matrix $\boldsymbol{G}_m^{(\mathcal{L})}$. The pseudocode for the maximization of these two cost functions is given in Algorithm 1.

Algorithm 1. Greedy algorithm.

Input : M matrices $\boldsymbol{G}_m^{(\mathcal{N})}$, the set of available radar positions $\mathcal{N}$, the number of radar positions to be selected L, and function $F(\cdot)$ (from (7) or (10)).
Output : Positions of L radars.
Initialize: The radar set, $\mathcal{I}$.
1. For (weighted) FP cost function:
   $\mathcal{I} = \arg\min_{i,j\in\mathcal{N}} \sum_{m=1}^{M} p_m \left|\mathrm{tr}\left\{\boldsymbol{G}_m^{(i)}\boldsymbol{G}_m^{(j)\dagger}\right\}\right|^2$.
2. For (weighted) LD cost function:
   $\mathcal{I} = \arg\max_{i\in\mathcal{N}} F(\boldsymbol{G}_m^{(i)})$.

Repeat : Until L positions are found
1. Find the radar $i = \arg\max_{i\notin\mathcal{I}} F(\mathcal{I}\cup i)$.
2. Update $\mathcal{I}$: $\mathcal{I} = \mathcal{I}\cup i$
3. For (weighted) FP cost function:
   (a) If $|\mathcal{I}| = N - L$, stop.
   (b) Assign the set of selected positions $\mathcal{L} = \mathcal{N}\backslash\mathcal{I}$.
4. For (weighted) LD cost function:
   (a) If $|\mathcal{I}| = L$, stop.
   (b) Assign the set of selected positions $\mathcal{L} = \mathcal{I}$.

3. Estimation of multi-modal parameters

Without loss of generality, let us consider a model, where the parameter vector $\boldsymbol{\alpha}$ is represented by two modalities. Examples of such a model are combinations of the simultaneous estimation of target range, radial velocity, and bearing in a single radar. Basically, the parameter vector for each grid point m from the parameter space is composed of two vectors with different measurement units $\boldsymbol{\alpha}_m = [\boldsymbol{\alpha}_{m,1}, \boldsymbol{\alpha}_{m,2}]^T$, where $\boldsymbol{\alpha}_{m,1} \in \mathbb{R}^{K_1}$ and $\boldsymbol{\alpha}_{m,2} \in \mathbb{R}^{K_2}$, with the total number of parameters under estimation given by $K = K_1 + K_2$. This also results in a splitting of the system matrix $\boldsymbol{G}_m^{(\mathcal{N})}$ as $\boldsymbol{G}_m^{(\mathcal{N})} = \left[\boldsymbol{G}_{m,1}^{(\mathcal{N})}, \boldsymbol{G}_{m,2}^{(\mathcal{N})}\right]$ with $\boldsymbol{G}_{m,1}^{(\mathcal{N})} \in \mathbb{R}^{QN\times K_1}$ and $\boldsymbol{G}_{m,2}^{(\mathcal{N})} \in \mathbb{R}^{QN\times K_2}$.

The MSE is then expressed as:

$$\mathrm{MSE} = \mathrm{E}(\|\boldsymbol{\alpha}_{m,1} - \hat{\boldsymbol{\alpha}}_{m,1}\|_2^2) + \mathrm{E}(\|\boldsymbol{\alpha}_{m,2} - \hat{\boldsymbol{\alpha}}_{m,2}\|_2^2). \tag{11}$$

However, since $\boldsymbol{\alpha}_{m,1}$ and $\boldsymbol{\alpha}_{m,2}$ represent different modalities, their errors should be treated differently. Therefore, we would like to introduce the weighting coefficients $w_{m,1}$ and $w_{m,2}$ in the MSE, which allows us to put a different emphasis on each term:

$$\mathrm{MSE} = w_{m,1}\mathrm{E}(\|\boldsymbol{\alpha}_{m,1} - \hat{\boldsymbol{\alpha}}_{m,1}\|_2^2) + w_{m,2}\mathrm{E}(\|\boldsymbol{\alpha}_{m,2} - \hat{\boldsymbol{\alpha}}_{m,2}\|_2^2). \tag{12}$$

This can be implicitly realized by rewriting the model in (2) as

$$\mathbf{y} \approx \mathbf{f}(\boldsymbol{\alpha}_m) + \widetilde{\boldsymbol{G}}_m^{(\mathcal{N})}(\tilde{\boldsymbol{\alpha}} - \tilde{\boldsymbol{\alpha}}_m) + \boldsymbol{\xi}, \tag{13}$$

where $\widetilde{\boldsymbol{G}}_m^{(\mathcal{N})}$ is the modified weighted matrix:

$$\widetilde{\boldsymbol{G}}_m^{(\mathcal{N})} = \left[\frac{1}{\sqrt{w_{m,1}}} \boldsymbol{G}_{m,1}^{(\mathcal{N})}, \frac{1}{\sqrt{w_{m,2}}} \boldsymbol{G}_{m,2}^{(\mathcal{N})} \right], \tag{14}$$

and where $\tilde{\boldsymbol{\alpha}}_m = \left[\sqrt{w_{m,1}}\boldsymbol{\alpha}_{m,1}, \sqrt{w_{m,2}}\boldsymbol{\alpha}_{m,2} \right]^T$ is the weighted parameter vector. Using the model (13) in the submodular costs (7) and (10) will implicitly relate these costs to the weighted MSE (12). The possibility to operate with the weights p_m, $w_{m,1}$, and $w_{m,2}$ expands the set of application scenarios for topology optimization of radar networks. For example, the radar network topology can be optimized for scenarios, where some grid points from the parameter space are uni-modal, while others are multi-modal.

4. Topology optimization of the FMCW radar network

4.1. System model

We consider a 3D scenario with N widely distributed potential positions of the radar nodes. These nodes are assumed to be monostatic FMCW radars that explore the autonomous mode of the signal transmission–reception (see Fig. 1). Each FMCW radar transmits a burst of the linear frequency-modulated (LFM) pulses that can be represented by:

$$x^{(n)}(t) = A_0 \exp\left(jt\left[\omega_c + \mathrm{frac}\left(\frac{t}{T_s} \right)\Delta\omega \right] \right), \tag{15}$$

where $A_0 = |A_0| \exp(j\varphi_0)$ is the transmit signal amplitude, $\omega_c = 2\pi f_c$ with f_c being the signal center frequency, $\Delta\omega = 2\pi\Delta f$ with Δf being the signal bandwidth, $n = 1, \ldots, N$, and T_s the sweep time. Note that the data association problem that arises in scenarios with multiple targets is not considered in this paper. It is assumed that the signals from different targets are properly associated in the preceding data processing step.

The signal reflected from the moving target related to the mth grid point is shifted in time and frequency as

$$y_m^{(n)}(t) = A_m^{(n)} x^{(n)}(t - \tau_m^{(n)}) \exp(-j(t - \tau_m^{(n)})\omega_{d_m}^{(n)}) + \xi^{(n)}(t), \tag{16}$$

where $A_m^{(n)} = |A_m^{(n)}| \exp(j\varphi_m^{(n)})$ is the non-fluctuating amplitude of the received signal; $\tau_m^{(n)}$ is the signal time delay related to the target-radar distance $R_m^{(n)}$

$$R_m^{(n)} = \sqrt{(x_m - x^{(n)})^2 + (y_m - y^{(n)})^2 + (z_m - z^{(n)})^2}$$

as $\tau_m^{(n)} = 2R_m^{(n)}/c$ with c being the speed of light; $(x_m,\ y_m,\ z_m)$ and $(x^{(n)},\ y^{(n)},\ z^{(n)})$ are the target and the nth radar coordinates respectively; $\omega_{d_m}^{(n)} = 2\pi f_{d_m}^{(n)}$ with $f_{d_m}^{(n)}$ being the Doppler frequency of the received signal, which is related to the radial target velocity $v_{r_m}^{(n)} = (v_{x_m}(x_m - x^{(n)}) + v_{y_m}(y_m - y^{(n)}) + v_{z_m}(z_m - z^{(n)}))/R_m^{(n)}$ (v_{x_m}, v_{y_m}, and v_{z_m} are the projections of the target velocity $\boldsymbol{v}_m$ on the x-, y-, and z-axes) as $\omega_{d_m}^{(n)} = 2\omega_c v_{r_m}^{(n)}/c$; $\xi(t)^{(n)}$ is a zero-mean i.i.d. Gaussian noise with variance σ^2. Following the model (1), we define $f^{(n)}(t; \boldsymbol{\alpha}_m) = |A_m^{(n)}| \exp(j\varphi_m^{(n)}) \exp(-j(t - \tau_m^{(n)})\omega_{d_m}^{(n)}) x^{(n)}(t - \tau_m^{(n)})$ and obtain

$$y_m^{(n)}(t) = f^{(n)}(t; \boldsymbol{\alpha}_m) + \xi^{(n)}(t), \tag{17}$$

where $\boldsymbol{\alpha}_m = [x_m,\ y_m,\ z_m,\ v_{x_m},\ v_{y_m},\ v_{z_m}]^T$.

In this scenario, we assume that the target location and velocity vector estimation is realized via a two-step de-centralized approach. In the first step, the target detection and the estimation of the time delay and Doppler frequency are done in a single radar, based on the echo-signal reflected from the target. In the second step, these local measurements are transferred to the central processing unit (CPU), where the estimation of the target position and/or velocity vectors is performed. In order to simplify the evaluation of the FP and the LD cost functions, first we evaluate the estimation performance of the target range and radial velocity for a single FMCW radar. Next, we introduce the closed-form expressions, based on a single radar node performance, for the evaluation of these FP and LD costs.

4.2. The performance of a single FMCW radar

Assuming a fixed sampling frequency that results in Q accumulated signal samples per integration time DT_s in each radar, the measurement model for a single radar is then given by (1) for $N = 1\left(\mathcal{N} = \{1\}\right)$. We linearize the noiseless signal $\boldsymbol{f}(\boldsymbol{\alpha}_m)$ around the parameter vector $\boldsymbol{\beta}_m = [\beta_{m,1},\ \beta_{m,2}]^T$ with $J=2$ components, $\beta_{m,1} = \tau_m$ and $\beta_{m,2} = \omega_{d_m}$. The matrix $\boldsymbol{G}_m^{(1)} \in \mathbb{R}^{Q\times J}$ is then given by $\left[\boldsymbol{G}_m^{(1)}\right]_{q,j} = \frac{\partial f_q(\boldsymbol{\alpha}_m)}{\partial \beta_{m,j}} \frac{1}{\sqrt{w_{m,j}}}$ ($j = 1, \ldots, J$) with

$$\frac{\partial f_q(\boldsymbol{\alpha}_m)}{\partial \beta_{m,1}} = -j|A_m^{(1)}| \left[\omega_c + 2\mathrm{frac}\left(\frac{t_q - \tau_m^{(1)}}{T_s} \right)\Delta\omega - \omega_{d_m}^{(1)} \right] \times e^{j(t_q - \tau_m^{(1)})\left[\omega_c + \mathrm{frac}\left(\frac{t_q - \tau_m^{(1)}}{T_s}\right)\Delta\omega - \omega_{dm}^{(1)}\right] + j\varphi_m^{(1)}};$$

$$\frac{\partial f_q(\boldsymbol{\alpha}_m)}{\partial \beta_{m,2}} = -j\left|A_m^{(1)}\right|\left(t_q - \tau_m^{(1)}\right) e^{j(t_q - \tau_m^{(1)})\left[\omega_c + \mathrm{frac}\left(\frac{t_q - \tau_m^{(1)}}{T_s}\right)\Delta\omega - \omega_{dm}^{(1)}\right] + j\varphi_m^{(1)}}.$$

We define the performance of a single radar that characterizes the estimation accuracy of the time delay and Doppler frequency of the signal, reflected from the target represented by the mth grid point from the parameter space, as

$$P_m^{(1)} = \mathrm{tr}\left\{ \boldsymbol{G}_m^{(1)} \boldsymbol{G}_m^{(1)\dagger} \right\} = P_m^{(1)}(\tau) + P_m^{(1)}(\omega_d) + 2P_m^{(1)}(\tau, \omega_d), \tag{18}$$

where

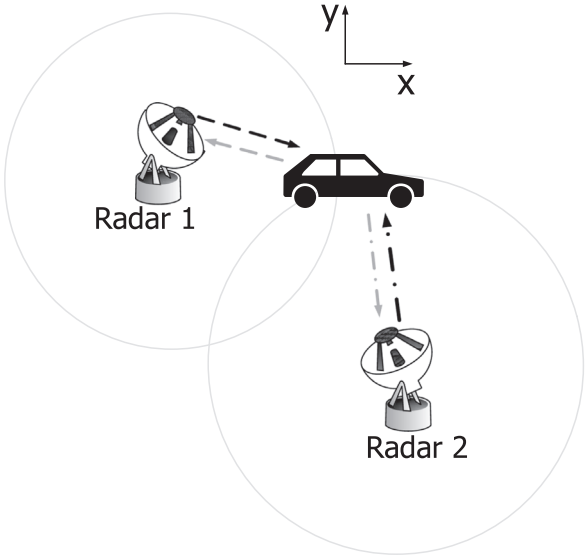

Fig. 1. Target localization in a monostatic radar network with autonomous signal reception.

$$P_m^{(1)}(\tau) = \frac{1}{w_{m,1}} \sum_{q=1}^{Q} \frac{\partial f_q(\boldsymbol{\alpha}_m)}{\partial \tau_m^{(1)}} \frac{\partial f_q^*(\boldsymbol{\alpha}_m)}{\partial \tau_m^{(1)}} = \frac{4}{3} \frac{1}{w_{m,1}} \Delta\omega^2 |A_m^{(1)}|^2 Q;$$

$$P_m^{(1)}(\omega_d) = \frac{1}{w_{m,2}} \sum_{q=1}^{Q} \frac{\partial f_q(\boldsymbol{\alpha}_m)}{\partial \omega_{d_m}^{(1)}} \frac{\partial f_q^*(\boldsymbol{\alpha}_m)}{\partial \omega_{d_m}^{(1)}} = \frac{1}{3} \frac{1}{w_{m,2}} T_s^2 D^2 |A_m^{(1)}|^2 Q;$$

$$P_m^{(1)}(\tau, \omega_d) = \frac{1}{\sqrt{w_{m,1} w_{m,2}}} \sum_{q=1}^{Q} \frac{\partial f_q(\boldsymbol{\alpha}_m)}{\partial \tau_m^{(1)}} \frac{\partial f_q^*(\boldsymbol{\alpha}_m)}{\partial \omega_{d_m}^{(1)}} = \frac{1}{\sqrt{w_{m,1} w_{m,2}}} \Delta\omega D T_s |A_m^{(1)}|^2 Q; \tag{19}$$

with $w_{m,1}$ and $w_{m,2}$ being the weighting coefficients.

4.3. The FP and the LD cost functions for an FMCW radar network

The measurement model for the radar network is given by (1). The parameter vector is the target state vector that contains two different modalities: target position and velocity. Thus, we define $\tilde{\boldsymbol{\alpha}}_m = \left[\sqrt{w_{1,m}}\boldsymbol{\alpha}_{m,1}, \sqrt{w_{2,m}}\boldsymbol{\alpha}_{m,2}\right]^T$, where $\boldsymbol{\alpha}_{m,1} = [x_m, y_m, z_m]^T$ and $\boldsymbol{\alpha}_{m,2} = [v_{x_m}, v_{y_m}, v_{z_m}]^T$ with $K_1 = 3$ and $K_2 = 3$ components, respectively. The weighted linear system matrix $\widetilde{\boldsymbol{G}}_m^{(\mathcal{N})} \in \mathbb{R}^{NQ \times (K_1+K_2)}$ consists of two submatrices $\boldsymbol{G}_{m,1}^{(\mathcal{N})}$ and $\boldsymbol{G}_{m,2}^{(\mathcal{N})}$, which are defined as

$$\left[\boldsymbol{G}_{m,1}^{(\mathcal{N})}\right]_{(n-1)Q+q,d} = \frac{\partial f_{(n-1)Q+q}(\tilde{\boldsymbol{\alpha}}_m)}{\partial \beta_{m,1}} \frac{\partial \beta_{m,1}}{\partial [\boldsymbol{\alpha}_{m,1}]_d} \frac{1}{\sqrt{w_{m,1}}} + \frac{\partial f_{(n-1)Q+q}(\tilde{\boldsymbol{\alpha}}_m)}{\partial \beta_{m,2}} \frac{\partial \beta_{m,2}}{\partial [\boldsymbol{\alpha}_{m,1}]_d} \frac{1}{\sqrt{w_{m,2}}};$$

$$\left[\boldsymbol{G}_{m,2}^{(\mathcal{N})}\right]_{(n-1)Q+q,b} = \frac{\partial f_{(n-1)Q+q}(\tilde{\boldsymbol{\alpha}}_m)}{\partial \beta_{m,2}} \frac{\partial \beta_{m,2}}{\partial [\boldsymbol{\alpha}_{m,2}]_b} \frac{1}{\sqrt{w_{m,2}}};$$

with $d = 1, \ldots, K_1$ and $b = 1, \ldots, K_2$.

The LD and the FP for the FMCW radar network can then be evaluated as

$$\mathrm{LD}(\mathcal{L}) = \sum_{m=1}^{M} p_m \left(\log\det\left(\sum_{i \in \mathcal{L}} \boldsymbol{T}_m^{(i)} + \epsilon \mathbf{I}_K \right)^{-1} + K \log \epsilon \right), \tag{20}$$

$$\mathrm{FP}(\mathcal{L}) = \sum_{m=1}^{M} p_m \sum_{i,j \in \mathcal{L}} \boldsymbol{S}_m^{(i,j)}, \tag{21}$$

where $\boldsymbol{T}_m^{(i)} = \widetilde{\boldsymbol{G}}_m^{(i)\dagger} \widetilde{\boldsymbol{G}}_m^{(i)}$, $\boldsymbol{S}_m^{(i,j)} = \sum_{n=1,l=1}^{K} \left[\boldsymbol{T}_m^{(i)}\right]_{n,l} \left[\boldsymbol{T}_m^{(j)}\right]_{n,l}$. The closed-form expressions for the entries of the matrix $\boldsymbol{T}_m^{(i)}$ are provided in Appendix A.

5. Numerical results

In this section, we apply the developed framework for the selection of the L most favorable positions of short-range FMCW monostatic radars in terms of the minimum MSE of the target parameter vector estimates. The estimation of the target position has to be performed over the area of the TU-Delft campus (dimension is approx. 400 000 m^2), which is represented by a uniform grid with a cell size of 50 m^2 ($M = 171$). The potential radar positions are represented by $N = 117$ non-uniformly distributed nodes (Fig. 2). These positions are selected such that radars can be located on the roofs of the buildings in a 3D spatial model. The parameters of a single radar node are presented in Table 1. The target maximal radar cross-section (RCS) is 1 m^2. A free-space propagation model is considered in this simulation. This model is based on the assumption that the first and strongest signal component in time corresponds to the line-of-sight propagation.

Two measurement models are considered: 1) range estimation for target localization and 2) simultaneous range and radial velocity estimation for target position and velocity vector estimation.

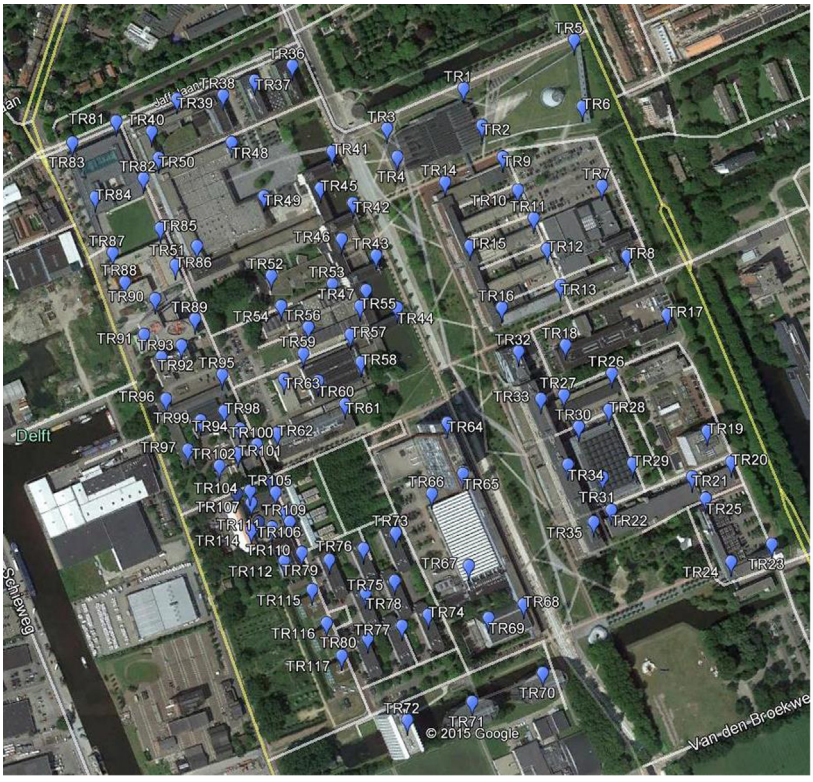

Fig. 2. Candidate radar positions for the TU-Delft campus. The area dimension is approx. 400 000 m^2.

In each of the scenarios considered in this section, we put equal weights on the grid points from the parameter space, i.e., $p_m = 1/M$.

First, we consider the scenario, where the spatial positions of the radar nodes need to be optimized in order to provide an accurate estimation of the 2D target position. The potential positions of the radar nodes are modeled in a 2D plane as well. In this simulation, we compare three performance metrics: the frame potential, the log-determinant, and the maximum eigenvalue of the error covariance matrix ($\lambda_{\max}$). While the first two costs are optimized using a greedy approach, the third one, $\lambda_{\max}$, is exploited in the convex optimization algorithm that can be found in [11]. The dependence of the average RMSE on the number of selected radars L for the three costs is shown in Fig. 3. The LD cost function leads to more favorable radar network geometries in terms of average RMSE, compared to the FP. Moreover, it allows for a better or equivalent estimation accuracy, compared to the $\lambda_{\max}$-driven optimization. Additionally, the linear complexity of the greedy algorithms in terms of N signifies the advantage of the LD over other cost functions. The overlap of the curves for a large L is caused by the high density of the radar grid relative to the size of the target area. The contour plot of the RMSE distribution for $L=20$ optimally placed radars using the log-determinant cost function demonstrates a high localization accuracy in the area of interest (see Fig. 4).

Next, we consider a scenario, where a 2D position estimation of a ground target and a 3D position and velocity estimation of a low-level airspace target has to be performed. Such a scenario might occur in multifunctional radar network operations, where surveillance of ground-based targets is combined with the tracking of low-altitude flying targets. The parameter space consists of two subspaces. In the first subspace, the parameter vector has two components (2D target position); in the second subspace, the parameter vector has three components (3D target position and velocity). The first subspace is represented by the $M_1 = 171$ grid points that have been used in the previous analysis for the TU-Delft campus area representation. In the second subspace, the target horizontal coordinates (x_m, y_m) are the same as in the first scenario, while the vertical coordinate z_m can take values $\{100, 200, \ldots, 1500\}$ m. Additionally, the target velocity can take any value from the velocity domain, represented by the set of target velocity values $v = \{2,\ 6,\ 10,\ 14,\ 18,\ 22\}$ m/s and movement directions in azimuth $\phi = \{0,\ \pi/4,\ \pi/2,\ 3\pi/4,\ \pi,\ 5\pi/4,\ 3\pi/2,\ 7\pi/4\}$ and elevation $\rho = \{-\pi/2,\ -\pi/4,\ \pi,\ \pi/4,\ \pi/2\}$, respectively (see Fig. 5). Consequently, each position grid point is assigned with $6 \times 8 \times 5 = 240$ possible velocities in the second scenario which results in $M_2 = 240 \times 15 \times 171 = 615\,600$ grid points. As one can see, the use of the target velocity is cumbersome. An interesting direction for further research can be the investigation of more practical algorithms to handle such large amounts of target grid points. In this simulation, we assume that the altitudes of the radar nodes are equal to 20 m each, which corresponds to the average height of the buildings on the TU-Delft campus.

The lower bounds on the variances of the time delay and Doppler frequency estimation are given by [26]:

$$\sigma_{\tau\tau}^2 \approx \frac{3}{2}\frac{1}{\Delta\omega^2\ \mathrm{SNR}}, \tag{22}$$

$$\sigma_{\omega_d\omega_d}^2 \approx \frac{6}{T_s^2\ D^2\ \mathrm{SNR}}, \tag{23}$$

where the signal-to-noise ratio is evaluated from the radar equation

$$\mathrm{SNR} = \frac{P_t G_a^2 \mathrm{RCS} T_s}{(4\pi)^3 f_c R^4 L_{syst} k_B T_{syst}} G_{proc}, \tag{24}$$

with P_t being the transmitted power, G_a the antenna gain, L_{syst} the system loss, T_{syst} the system temperature, G_{proc} the processing gain, and k_B the Boltzmann constant. For a single radar with parameters listed in Table 1, the accuracy of time delay estimation will be eight times worse than the accuracy of Doppler frequency estimation. As a result, the weighting coefficients are chosen as $w_{m,1} = 1$ and $w_{m,2} = 64$.

Table 1
Single radar simulation parameters.

Parameter	Value
ERP $[P_t G_a]$	10 dBm
Carrier frequency $[f_c]$	25 GHz
Sweep time $[T_s]$	$0.5{\cdot}10^{-3}$ s
Number of integrated pulses [D]	512
Signal bandwidth $[\Delta f]$	250 MHz
Receiver bandwidth $[B]$	300 kHz
Noise figure $[F_n]$	8 dB
System losses $[L_{syst}]$	15 dB

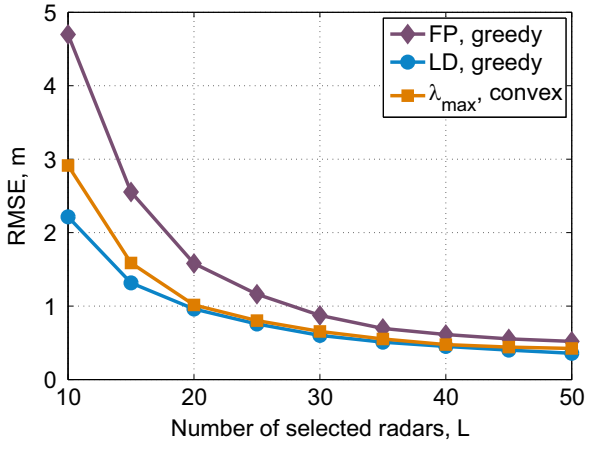

Fig. 3. Average RMSE of the target localization for different numbers of optimally placed radars L from the $N=117$ available ones for the $K=2$ parameters under estimation and the $M=171$ grid points for the parameter space.

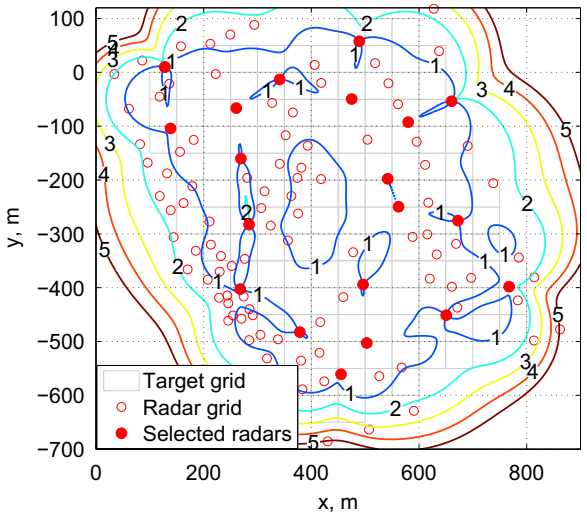

Fig. 4. Contour plot of the RMSE (m) of the target localization with $L = 20$ optimally sited short-range FMCW radars using the greedy algorithm based on a log-determinant cost function.

Fig. 6 shows the dependence of the RMSEs of the position (Fig. 6a) and the velocity (Fig. 6b) estimates as a function of L for both the FP and the LD cost functions. For this scenario, the LD cost function again outperforms the FP. Compared to the previous scenario (Fig. 3), the RMSE curves for the FP and the LD cost functions do not coincide with increasing the number of selected radars L. This is due to the large parameter space with most of the grid points lying above the radar grid. The latter leads to a lower SNR and worse estimation performance. This scenario is aimed to show the capability to perform topology optimization of multi-functional radar systems. Moreover, scenarios with different sensor types can be considered as a further extension of this work.

5.1. The influence of the weighting coefficients

Finally, we compare the topology selection results in terms of RMSE of the target position estimation for two measurement models of a single radar: (1) only target range measurement; (2) target range and radial velocity measurement. The first measurement model implies only target localization, while the second one implies both target localization and velocity estimation in the radar network. In the second measurement model, it is assumed that both range and radial velocity are used for target localization. In order to investigate the effect of the target movement on the localization accuracy, three scenarios of target movement are considered (Fig. 7): (a) along the y-axis (Scenario 1); (b) along the x-axis (Scenario 2); (c) at an angle of 45° from the x- and the y-axes (Scenario 3). The target velocity is $v = 10$ m/s. Fig. 8 presents the ratios of the positioning RMSEs ($\mathrm{RMSE_p}$) for two measurement models, $L=10$ selected radar positions and different values of the weighting coefficients. The superscript index in the RMSE specifies the measurement model, i.e., either the first or the second one. As apparent from the results, the effect of the weights and the measurement model itself for the three scenarios is dissimilar. First of all, localization-driven topology optimization, in general, can outperform the location- and velocity-driven topology optimization (the first and the third scenario of the target movement) in terms of the RMSE of target localization. This is not the case for the second movement scenario, where the selected topologies based on the second measurement model result in a lower RMSE for all considered values of the weighting coefficients $w_{m,1}$ and $w_{m,2}$. Second, using the best weighting coefficients, we can achieve up to 3 dB improvement in terms of the localization RMSE. At last, when no weights are introduced ($w_{m,1} = 1$ and $w_{m,2} = 1$), the location- and velocity-driven topology optimization allows for a better or equivalent performance compared to only localization-driven topology optimization. Fig. 9 shows two network topologies for two measurement models and three different scenarios. As one can see, the difference between the optimal topologies for the two measurement models can be up to six radar node positions, which results in a different estimation accuracy. In each of the considered scenarios, the optimal topologies correspond to those that enclose the target areas.

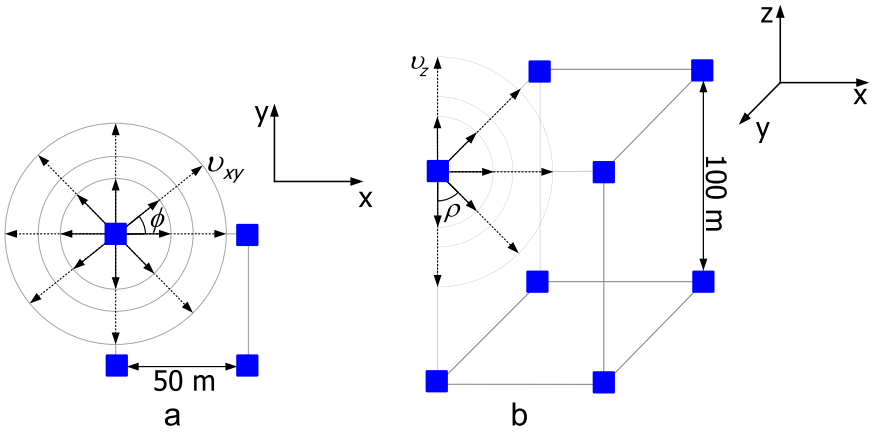

Fig. 5. Gridding of the velocity domain (squares are the grid points that represent the target area). (a) In azimuth, (b) in elevation.

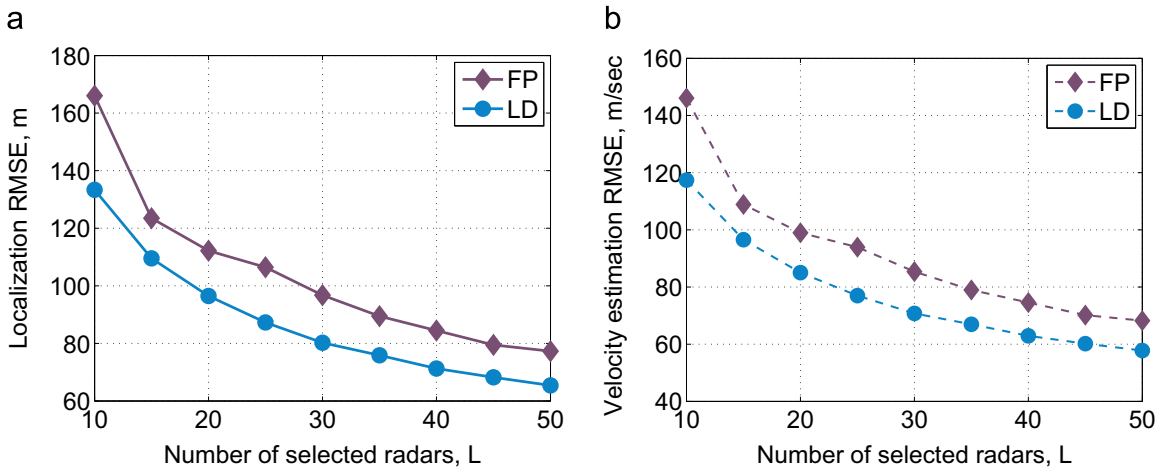

Fig. 6. Average RMSE of the target position and velocity for different numbers of optimally placed radars L for a 2D position estimation and a 3D position+velocity estimation. (a) Position accuracy, (b) velocity accuracy.

5.2. Computational complexity

Both the FP and the LD cost functions explore the greedy Algorithm 1. The complexity of the greedy Algorithm 1 for the weighted log-det cost function is linear with respect to the number of potential radar node positions N, $O(N)$, since N matrices are evaluated in Algorithm 1. For the weighted frame potential the complexity of the same algorithm is cubic with respect to N, $O(N^3)$. This is related to the fact that for each of the $N-L$ steps, there are $(N-S)^2$ terms ($S=3, \ldots, (N-L)$). The complexity of the algorithm can be further reduced to $O(N^2)$ by exploiting the recursive property of the FP function. Based on this, for large-scale problems with $L \ll N$ and $K \ll N$, the LD cost function allows for a lower computational complexity, compared to the FP cost function. At the same time, Algorithm 1 for the LD cost is cubic in the number of parameters under estimation K, $O(K^3)$, while for the FP it is linear in K, $O(K)$. Therefore, exploiting the LD cost for problems where K is in the order of N would entail a higher complexity, compared to the FP.

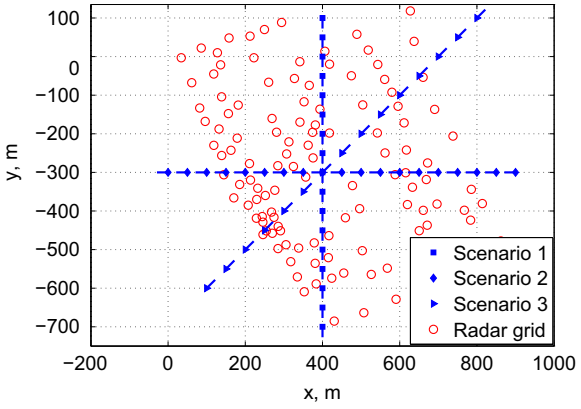

Fig. 7. Scenarios of the target movement. Line directions on the target grid points correspond to the target velocity vectors (not in scale).

6. Conclusions

In this paper, we have proposed a generic framework of radar network topology optimization, based on the greedy algorithm. The theory is developed for non-linear measurement models with an extension to the case of multi-modal parameter vector estimation. This approach can be applied for scenarios of temporal (measurements are done with one radar) as well as spatio-temporal (measurements are done with a radar network, where the data fusion on the level of signal samples takes place) data selection.

The developed framework has been applied to the optimal topology selection of radar nodes for the simultaneous position and velocity estimation of a target. The scenarios where different points from the parameter space can be represented with different modalities are feasible as well. Three cost functions were compared: the frame potential, the log-determinant and the maximum eigenvalue costs, with the last two being scalar functions of the error covariance matrix. The results show that the log-determinant and the maximum eigenvalue show an equivalent performance in terms of average RMSE, while the greedy optimization of the log-determinant is much more computationally efficient than the convex optimization of the maximum eigenvalue. Moreover, the performance of the location-driven versus the position- and velocity-driven optimization was compared, showing a further improvement in terms of average RMSE of the target parameter vector estimation, when the target movement is taken into account.

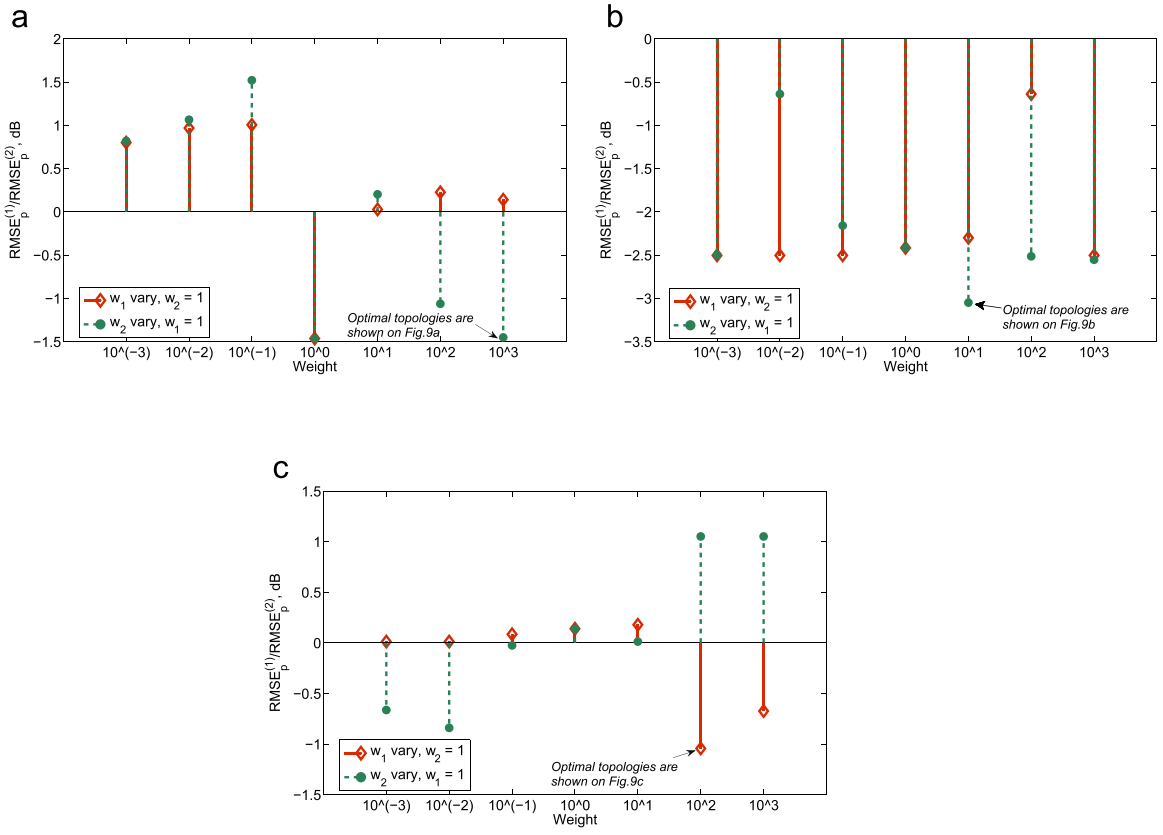

Fig. 8. Ratios of the RMSEs of the target localization for optimal radar network topologies for two measurement models at $L = 10$: (1) the range estimation for target localization; (2) the range and radial velocity estimation for target location and velocity vectors estimation. (a) Scenario 1: $v_x = 0$, $v_y = v$, (b) Scenario 2: $v_x = v$, $v_y = 0$, (c) Scenario 3: $v_x = v_y$.

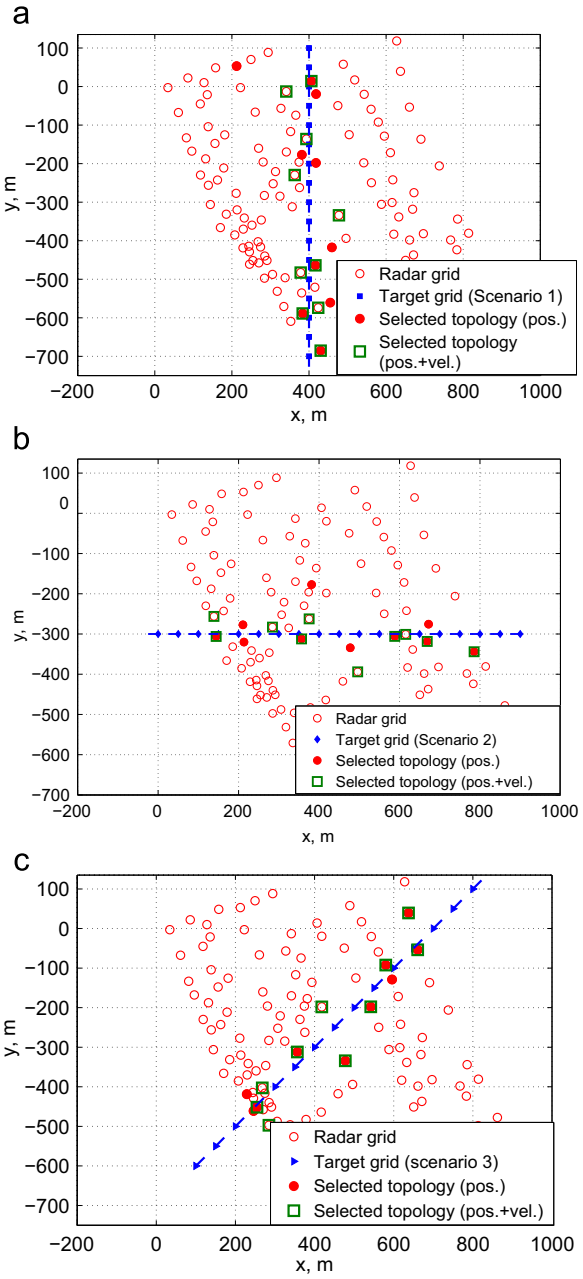

Fig. 9. Selected topologies of the radar networks for target localization only and for target location + velocity estimation. (a) Scenario 1: $w_{m,1}=1,\ w_{m,2}=10^3$, (b) Scenario 2: $w_{m,1}=1,\ w_{m,2}=10$, (c) Scenario 3: $w_{m,1}=10^2,\ w_{m,2}=1$.

Acknowledgments

This research was partly supported by the Raebell project.

Appendix A. The evaluation of the FP and LD in (21) and (22)

In this appendix, we provide the closed-form expressions for the evaluation of the matrix $\boldsymbol{T}_m^{(i)}=\widetilde{\boldsymbol{G}}_m^{(i)\dagger}\widetilde{\boldsymbol{G}}_m^{(i)}$ with $\widetilde{\boldsymbol{G}}_m^{(i)}=\left[\frac{1}{\sqrt{w_{m,1}}}\boldsymbol{G}_{m,1}^{(i)},\frac{1}{\sqrt{w_{m,2}}}\boldsymbol{G}_{m,2}^{(i)}\right]$ being the weighted linear system matrix in the scenario of (multi-modal) target state vector estimation. The matrices $\boldsymbol{G}_{m,1}^{(i)}\in\mathbb{R}^{Q\times K_1}$ and $\boldsymbol{G}_{m,2}^{(i)}\in\mathbb{R}^{Q\times K_2}$ are defined as $\left[\boldsymbol{G}_{m,1}^{(i)}\right]_{q,d}=\frac{\partial f_q(\tilde{\boldsymbol{\alpha}}_m)}{\partial\beta_{m,1}}\frac{\partial\beta_{m,1}}{\partial[\boldsymbol{\alpha}_{m,1}]_d}\frac{1}{\sqrt{w_{m,1}}}+\frac{\partial f_q(\tilde{\boldsymbol{\alpha}}_m)}{\partial\beta_{m,2}}\frac{\partial\beta_{m,2}}{\partial[\boldsymbol{\alpha}_{m,1}]_d}\frac{1}{\sqrt{w_{m,2}}}$ and $\left[\boldsymbol{G}_{m,2}^{(i)}\right]_{q,b}=\frac{\partial f_q(\tilde{\boldsymbol{\alpha}}_m)}{\partial\beta_{m,2}}\frac{\partial\beta_{m,2}}{\partial[\boldsymbol{\alpha}_{m,2}]_b}\frac{1}{\sqrt{w_{m,2}}}$ with $d=1,\ldots,K_1$ and $b=1,\ldots,K_2$. The parameter vector is $\tilde{\boldsymbol{\alpha}}_m=\left[\sqrt{w_{m,1}}\boldsymbol{\alpha}_{m,1},\sqrt{w_{m,2}}\boldsymbol{\alpha}_{m,2}\right]^T$ with $\boldsymbol{\alpha}_{m,1}=[x_m,\ y_m,\ z_m]^T$ and $\boldsymbol{\alpha}_{m,2}=[v_{x_m},\ v_{y_m},\ v_{z_m}]^T$.

The matrix $\boldsymbol{T}_m^{(i)}$ can be then evaluated as

$$\left[\boldsymbol{T}_m^{(i)}\right]_{11}=P_m^{(i)}(\tau)\left(\frac{\partial\tau_m^{(i)}}{\partial x_m}\right)^2+P_m^{(i)}(\omega_d)\left(\frac{\partial\omega_{d_m}^{(i)}}{\partial x_m}\right)^2+2P_m^{(i)}(\tau,\omega_d)\frac{\partial\tau_m^{(i)}}{\partial x_m}\frac{\partial\omega_{d_m}^{(i)}}{\partial x_m};$$

$$\left[\boldsymbol{T}_m^{(i)}\right]_{12}=\left[\boldsymbol{T}_m^{(i)}\right]_{21}=P_m^{(i)}(\tau)\frac{\partial\tau_m^{(i)}}{\partial x_m}\frac{\partial\tau_m^{(i)}}{\partial y_m}+P_m^{(i)}(\tau,\omega_d)\frac{\partial\tau_m^{(i)}}{\partial x_m}\frac{\partial\omega_{d_m}^{(i)}}{\partial y_m}+P_m^{(i)}(\tau,\omega_d)\frac{\partial\tau_m^{(i)}}{\partial y_m}\frac{\partial\omega_{d_m}^{(i)}}{\partial x_m}+P_m^{(i)}(\omega_d)\frac{\partial\omega_{d_m}^{(i)}}{\partial x_m}\frac{\partial\omega_{d_m}^{(i)}}{\partial y_m};$$

$$\left[\boldsymbol{T}_m^{(i)}\right]_{13}=\left[\boldsymbol{T}_m^{(i)}\right]_{31}=P_m^{(i)}(\tau)\frac{\partial\tau_m^{(i)}}{\partial x_m}\frac{\partial\tau_m^{(i)}}{\partial z_m}+P_m^{(i)}(\tau,\omega_d)\frac{\partial\tau_m^{(i)}}{\partial x_m}\frac{\partial\omega_{d_m}^{(i)}}{\partial z_m}+P_m^{(i)}(\tau,\omega_d)\frac{\partial\tau_m^{(i)}}{\partial z_m}\frac{\partial\omega_{d_m}^{(i)}}{\partial x_m}+P_m^{(i)}(\omega_d)\frac{\partial\omega_{d_m}^{(i)}}{\partial x_m}\frac{\partial\omega_{d_m}^{(i)}}{\partial z_m};$$

$$\left[\boldsymbol{T}_m^{(i)}\right]_{14}=\left[\boldsymbol{T}_m^{(i)}\right]_{41}=P_m^{(i)}(\tau,\omega_d)\frac{\partial\tau_m^{(i)}}{\partial x_m}\frac{\partial\omega_{d_m}^{(i)}}{\partial v_{x_m}}+P_m^{(i)}(\omega_d)\frac{\partial\omega_{d_m}^{(i)}}{\partial x_m}\frac{\partial\omega_{d_m}^{(i)}}{\partial v_{x_m}};$$

$$\left[\boldsymbol{T}_m^{(i)}\right]_{15}=\left[\boldsymbol{T}_m^{(i)}\right]_{51}=P_m^{(i)}(\tau,\omega_d)\frac{\partial\tau_m^{(i)}}{\partial x_m}\frac{\partial\omega_{d_m}^{(i)}}{\partial v_{y_m}}+P_m^{(i)}(\omega_d)\frac{\partial\omega_{d_m}^{(i)}}{\partial x_m}\frac{\partial\omega_{d_m}^{(i)}}{\partial v_{y_m}};$$

$$\left[\boldsymbol{T}_m^{(i)}\right]_{16}=\left[\boldsymbol{T}_m^{(i)}\right]_{61}=P_m^{(i)}(\tau,\omega_d)\frac{\partial\tau_m^{(i)}}{\partial x_m}\frac{\partial\omega_{d_m}^{(i)}}{\partial v_{z_m}}+P_m^{(i)}(\omega_d)\frac{\partial\omega_{d_m}^{(i)}}{\partial x_m}\frac{\partial\omega_{d_m}^{(i)}}{\partial v_{z_m}};$$

$$\left[\boldsymbol{T}_m^{(i)}\right]_{22}=P_m^{(i)}(\tau)\left(\frac{\partial\tau_m^{(i)}}{\partial y_m}\right)^2+2P_m^{(i)}(\tau,\omega_d)\frac{\partial\tau_m^{(i)}}{\partial y_m}\frac{\partial\omega_{d_m}^{(i)}}{\partial y_m}+P_m^{(i)}(\omega_d)\left(\frac{\partial\omega_{d_m}^{(i)}}{\partial y_m}\right)^2;$$

$$\left[\boldsymbol{T}_m^{(i)}\right]_{23}=\left[\boldsymbol{T}_m^{(i)}\right]_{32}=P_m^{(i)}(\tau)\frac{\partial\tau_m^{(i)}}{\partial y_m}\frac{\partial\tau_m^{(i)}}{\partial z_m}+P_m^{(i)}(\tau,\omega_d)\frac{\partial\tau_m^{(i)}}{\partial y_m}\frac{\partial\omega_{d_m}^{(i)}}{\partial z_m}+P_m^{(i)}(\tau,\omega_d)\frac{\partial\tau_m^{(i)}}{\partial z_m}\frac{\partial\omega_{d_m}^{(i)}}{\partial y_m}+P_m^{(i)}(\omega_d)\frac{\partial\omega_{d_m}^{(i)}}{\partial y_m}\frac{\partial\omega_{d_m}^{(i)}}{\partial z_m};$$

$$\left[\boldsymbol{T}_m^{(i)}\right]_{24}=\left[\boldsymbol{T}_m^{(i)}\right]_{42}=P_m^{(i)}(\tau,\omega_d)\frac{\partial\tau_m^{(i)}}{\partial y_m}\frac{\partial\omega_{d_m}^{(i)}}{\partial v_{x_m}}+P_m^{(i)}(\omega_d)\frac{\partial\omega_{d_m}^{(i)}}{\partial y_m}\frac{\partial\omega_{d_m}^{(i)}}{\partial v_{x_m}};$$

$$\left[\boldsymbol{T}_m^{(i)}\right]_{25}=\left[\boldsymbol{T}_m^{(i)}\right]_{52}=P_m^{(i)}(\tau,\omega_d)\frac{\partial\tau_m^{(i)}}{\partial y_m}\frac{\partial\omega_{d_m}^{(i)}}{\partial v_{y_m}}+P_m^{(i)}(\omega_d)\frac{\partial\omega_{d_m}^{(i)}}{\partial y_m}\frac{\partial\omega_{d_m}^{(i)}}{\partial v_{y_m}};$$

$$\left[\boldsymbol{T}_m^{(i)}\right]_{26}=\left[\boldsymbol{T}_m^{(i)}\right]_{62}=P_m^{(i)}(\tau,\omega_d)\frac{\partial\tau_m^{(i)}}{\partial y_m}\frac{\partial\omega_{d_m}^{(i)}}{\partial v_{z_m}}+P_m^{(i)}(\omega_d)\frac{\partial\omega_{d_m}^{(i)}}{\partial y_m}\frac{\partial\omega_{d_m}^{(i)}}{\partial v_{z_m}};$$

$$\left[\boldsymbol{T}_m^{(i)}\right]_{33}=P_m^{(i)}(\tau)\left(\frac{\partial\tau_m^{(i)}}{\partial z_m}\right)^2+2P_m^{(i)}(\tau,\omega_d)\frac{\partial\tau_m^{(i)}}{\partial z_m}\frac{\partial\omega_{d_m}^{(i)}}{\partial z_m}+P_m^{(i)}(\omega_d)\left(\frac{\partial\omega_{d_m}^{(i)}}{\partial z_m}\right)^2;$$

$$\left[\boldsymbol{T}_m^{(i)}\right]_{34}=\left[\boldsymbol{T}_m^{(i)}\right]_{43}=P_m^{(i)}(\tau,\omega_d)\frac{\partial\tau_m^{(i)}}{\partial z_m}\frac{\partial\omega_{d_m}^{(i)}}{\partial v_{x_m}}+P_m^{(i)}(\omega_d)\frac{\partial\omega_{d_m}^{(i)}}{\partial z_m}\frac{\partial\omega_{d_m}^{(i)}}{\partial v_{x_m}};$$

$$\left[\boldsymbol{T}_m^{(i)}\right]_{35}=\left[\boldsymbol{T}_m^{(i)}\right]_{53}=P_m^{(i)}(\tau,\omega_d)\frac{\partial\tau_m^{(i)}}{\partial z_m}\frac{\partial\omega_{d_m}^{(i)}}{\partial v_{y_m}}+P_m^{(i)}(\omega_d)\frac{\partial\omega_{d_m}^{(i)}}{\partial z_m}\frac{\partial\omega_{d_m}^{(i)}}{\partial v_{y_m}};$$

$$\left[\boldsymbol{T}_m^{(i)}\right]_{36}=\left[\boldsymbol{T}_m^{(i)}\right]_{63}=P_m^{(i)}(\tau,\omega_d)\frac{\partial\tau_m^{(i)}}{\partial z_m}\frac{\partial\omega_{d_m}^{(i)}}{\partial v_{z_m}}+P_m^{(i)}(\omega_d)\frac{\partial\omega_{d_m}^{(i)}}{\partial z_m}\frac{\partial\omega_{d_m}^{(i)}}{\partial v_{z_m}};$$

$$\left[\boldsymbol{T}_m^{(i)}\right]_{44}=P_m^{(i)}(\omega_d)\left(\frac{\partial\omega_{d_m}^{(i)}}{\partial v_{x_m}}\right)^2;$$

$$\left[\boldsymbol{T}_m^{(i)}\right]_{45}=\left[\boldsymbol{T}_m^{(i)}\right]_{54}=P_m^{(i)}(\omega_d)\frac{\partial\omega_{d_m}^{(i)}}{\partial v_{x_m}}\frac{\partial\omega_{d_m}^{(i)}}{\partial v_{y_m}};$$

$$\left[\boldsymbol{T}_m^{(i)}\right]_{46}=\left[\boldsymbol{T}_m^{(i)}\right]_{64}=P_m^{(i)}(\omega_d)\frac{\partial\omega_{d_m}^{(i)}}{\partial v_{x_m}}\frac{\partial\omega_{d_m}^{(i)}}{\partial v_{z_m}};$$

$$\left[\boldsymbol{T}_m^{(i)}\right]_{55}=P_m^{(i)}(\omega_d)\left(\frac{\partial\omega_{d_m}^{(i)}}{\partial v_{y_m}}\right)^2;$$

$$\left[\boldsymbol{T}_m^{(i)}\right]_{56}=\left[\boldsymbol{T}_m^{(i)}\right]_{65}=P_m^{(i)}(\omega_d)\frac{\partial\omega_{d_m}^{(i)}}{\partial v_{y_m}}\frac{\partial\omega_{d_m}^{(i)}}{\partial v_{z_m}};$$

$$\left[\boldsymbol{T}_m^{(i)}\right]_{66}=P_m^{(i)}(\omega_d)\left(\frac{\partial\omega_{d_m}^{(i)}}{\partial v_{z_m}}\right)^2.$$

The derivatives of the time delay and the Doppler frequency with respect to target coordinates and velocities are:

$$\frac{\partial \tau_m^{(i)}}{\partial x_m} = \frac{2}{c}\frac{(x_m - x^{(i)})}{R_m^{(i)}};$$
$$\frac{\partial \tau_m^{(i)}}{\partial y_m} = \frac{2}{c}\frac{(y_m - y^{(i)})}{R_m^{(i)}};$$
$$\frac{\partial \tau_m^{(i)}}{\partial z_m} = \frac{2}{c}\frac{(x_m - x^{(i)})}{R_m^{(i)}}; \tag{25}$$

$$\frac{\partial \omega_{d_m}^{(i)}}{\partial x_m} = \frac{2\omega_c}{c}\frac{(R_m^{(i)})^2 v_{x_m} - b_m^{(i)}(x_m - x^{(i)})}{(R_m^{(i)})^3};$$
$$\frac{\partial \omega_{d_m}^{(i)}}{\partial y_m} = \frac{2\omega_c}{c}\frac{(R_m^{(i)})^2 v_{y_m} - b_m^{(i)}(y_m - y^{(i)})}{(R_m^{(i)})^3};$$
$$\frac{\partial \omega_{d_m}^{(i)}}{\partial z_m} = \frac{2\omega_c}{c}\frac{(R_m^{(i)})^2 v_{z_m} - b_m^{(i)}(z_m - z^{(i)})}{(R_m^{(i)})^3};$$
$$\frac{\partial \omega_{d_m}^{(i)}}{\partial v_{x_m}} = \frac{2\omega_0}{c}\frac{(x_m - x^{(i)})}{R_m^{(i)}};$$
$$\frac{\partial \omega_{d_m}^{(i)}}{\partial v_{y_m}} = \frac{2\omega_0}{c}\frac{(y_m - y^{(i)})}{R_m^{(i)}};$$
$$\frac{\partial \omega_{d_m}^{(i)}}{\partial v_{z_m}} = \frac{2\omega_0}{c}\frac{(z_m - z^{(i)})}{R_m^{(i)}}; \tag{26}$$

where $b_m^{(i)} = v_{x_m}(x_m - x^{(i)}) + v_{y_m}(y_m - y^{(i)}) + v_{z_m}(z_m - z^{(i)})$.

The matrix $\boldsymbol{T}_m^{(i)}$ can be easily truncated for the scenarios, where only target position or velocity is estimated. For example, for 3D target localization based on trilateration technique, the parameter vector is $\boldsymbol{\alpha}_m = [x_m, y_m, z_m]^T$. The entries of the measurement matrix $\boldsymbol{G}_{m,1}^{(i)} \in \mathbb{R}^{Q\times K_1}$ are then given by $\left[\boldsymbol{G}_{m,1}^{(i)}\right]_{q,d} = \frac{\partial f_q(\boldsymbol{\alpha}_m)}{\partial \beta_{m,1}}\frac{\partial \beta_{m,1}}{\partial [\boldsymbol{\alpha}_m]_d}$. The matrix $\boldsymbol{T}_m^{(i)} \in \mathbb{R}^{K_1\times K_1}$ can be evaluated at $w_{m,2} = 0$.

References

[1] D. Pepyne, D. McLaughlin, D. Westbrook, E. Lyons, E. Knapp, S. Frasier, M. Zink, Dense radar networks for low-flyer surveillance, in: 2011 IEEE International Conference on Technologies for Homeland Security (HST), 2011, pp. 413–418, http://dx.doi.org/10.1109/THS.2011.6107905.

[2] F. Folster, H. Rohling, U. Lubbert, An automotive radar network based on 77 GHz FMCW sensors, in: 2005 IEEE International Radar Conference, 2005, pp. 871–876, http://dx.doi.org/10.1109/RADAR.2005.1435950.

[3] R. Cardinali, E. Anniballi, C. Bongioanni, A. Macera, F. Colone, P. Lombardo, ARGUS 3D: security enhancements through innovative radar technologies, in: 2013 Eighth International Conference on Availability, Reliability and Security (ARES), 2013, pp. 759–765, http://dx.doi.org/10.1109/ARES.2013.101.

[4] V. Chernyak, Fundamentals of Multisite Radar Systems: Multistatic Radars and Multistatic Radar Systems, CRC Press Inc, Amsterdam, 1998.

[5] A.-S. Luce, H. Molina, D. Muller, V. Thirard, Experimental results on RIAS digital beamforming radar, in: Radar 92. International Conference, 1992, pp. 74–77.

[6] E. Hanle, Survey of bistatic and multistatic radar, IEE Proc. F – Commun. Radar Signal Process. 133 (7) (1986) 587–595, http://dx.doi.org/10.1049/ip-f-1.1986.0095.

[7] F. Robey, S. Coutts, D. Weikle, J. McHarg, K. Cuomo, MIMO radar theory and experimental results, in: 2004. Conference Record of the Thirty-Eighth Asilomar Conference on Signals, Systems and Computers, vol. 1, 2004, pp. 300–304, http://dx.doi.org/10.1109/ACSSC.2004.1399141.

[8] A. Di Lallo, A. Farina, R. Fulcoli, A. Stile, L. Timmoneri, D. Vigilante, A real time test bed for 2D and 3D multi-radar tracking and data fusion with application to border control, in: International Conference on Radar, 2006. CIE '06. 2006, pp. 1–6, http://dx.doi.org/10.1109/ICR.2006.343162.

[9] M. Skolnik, Radar Handbook, third edition, Electronics Electrical Engineering, McGraw-Hill Companies, Incorporated, New York, 2008.

[10] J. Li, P. Stoica, MIMO Radar Signal Processing, Wiley, Hoboken, New Jersey, 2008.

[11] S. Chepuri, G. Leus, Sparsity-promoting sensor selection for non-linear measurement models, IEEE Trans. Signal Process. 63 (3) (2015) 684–698, http://dx.doi.org/10.1109/TSP.2014.2379662.

[12] Q. He, R. Blum, D. Godrich, A. Haimovich, Target velocity estimation and antenna placement for MIMO radar with widely separated antennas, IEEE J. Sel. Top. Signal Process. 1 (4) (2010) 79–100, http://dx.doi.org/10.1109/JSTSP.2009.2038974.

[13] J. Ranieri, A. Chebira, M. Vetterli, Near-optimal sensor placement for linear inverse problems, IEEE Trans. Signal Process. 62 (5) (2014) 1135–1146, http://dx.doi.org/10.1109/TSP.2014.2299518.

[14] J. Isaacs, D. Klein, J. Hespanha, Optimal sensor placement for time difference of arrival localization, in: Proceedings of the 48th IEEE Conference on Decision and Control, 2009 held jointly with the 2009 28th Chinese Control Conference. CDC/CCC 2009, December, pp. 7878–7884. http://dx.doi.org/10.1109/CDC.2009.5399478.

[15] C.M. Hoyuela, A.J. Terzuoli, R.P. Wasky, Determining possible receiver locations for passive radar, IEE Proc. – Radar Sonar Navig. 152 (3) (2005) 206–214, http://dx.doi.org/10.1049/ip-rsn:20045023.

[16] P. Zhan, D. Casbeer, A. Swindlehurst, Adaptive mobile sensor positioning for multi-static target tracking, IEEE Trans. Aerosp. Electron. Syst. 46 (1) (2010) 120–132, http://dx.doi.org/10.1109/TAES.2010.5417151.

[17] X. Gong, J. Zhang, D. Cochran, When target motion matters: Doppler coverage in radar sensor networks, in: 2013 Proceedings IEEE INFOCOM, 2013, pp. 1169–1177, http://dx.doi.org/10.1109/INFCOM.2013.6566908.

[18] G. Gu, P. Chandler, C. Schumacher, A. Sparks, M. Pachter, Optimal cooperative sensing using a team of UAVs, IEEE Trans. Aerosp. Electron. Syst. 42 (4) (2006) 1446–1458, http://dx.doi.org/10.1109/TAES.2006.314584.

[19] T. Onel, C. Ersoy, H. Delic, Information content-based sensor selection and transmission power adjustment for collaborative target tracking, IEEE Trans. Mob. Comput. 8 (8) (2009) 1103–1116, http://dx.doi.org/10.1109/TMC.2009.12.

[20] H. Wang, G. Pottie, K. Yao, D. Estrin, Entropy-based sensor selection heuristic for target localization, in: Third International Symposium on Information Processing in Sensor Networks, 2004. IPSN 2004, 2004, pp. 36–45, http://dx.doi.org/10.1109/IPSN.2004.1307321.

[21] M. Shamaiah, S. Banerjee, H. Vikalo, Greedy sensor selection: leveraging submodularity, in: 2010 49th IEEE Conference on Decision and Control (CDC), 2010, pp. 2572–2577, http://dx.doi.org/10.1109/CDC.2010.5717225.

[22] I. Ivashko, O. Krasnov, A. Yarovoy, Sparsity-based optimization of the sensors positions in radar networks with separated transmit and receive nodes, Int. J. Distrib. Sensor Netw. (2016),http://dx.doi.org/10.1155/2016/9437602 Article ID 9437602, 10 pp.

[23] M. Fisher, G. Nemhauser, L. Wolsey, An analysis of approximations for maximizing submodular set functions, in: M. Balinski, A. Hoffman (Eds.), Polyhedral Combinatorics, Mathematical Programming Studies, vol. 8, Springer, Berlin, Heidelberg, 1978, pp. 73–87, http://dx.doi.org/10.1007/BFb0121195.

[24] D. El Badawy, J. Ranieri, M. Vetterli, Near-optimal sensor placement for signals lying in a union of subspaces, in: 2014 Proceedings of the 22nd European Signal Processing Conference (EUSIPCO), 2014, pp. 880–884.

[25] S. Rao, S. Chepuri, G. Leus, Greedy sensor selection for non-linear models, in: 2016 Proceedings of the 24th European Signal Processing Conference (EUSIPCO), 2016.

[26] I. Ivashko, O. Krasnov, A. Yarovoy, Performance analysis of multisite radar systems, in: 2013 European Microwave Conference (EuMC), 2013, pp. 1771–1774.